Understanding large-scale atmospheric and oceanic flows with layered rotating shallow water models

V. Zeitlin,

Non-homogeneous Fluids and Flows, Prague, August 2012

Plan

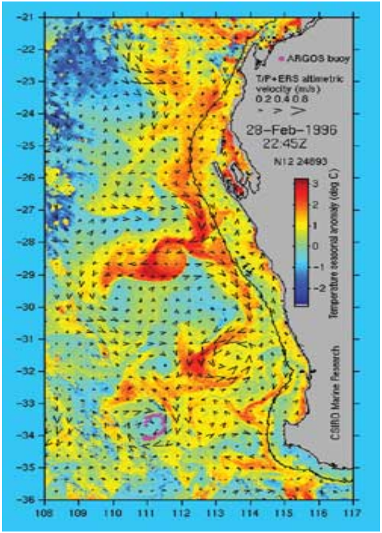
ARGOS buoy
T/P+ERS altimetric velocity (m/s)
0.2 0.4 0.8
28–Feb–1996
22:45Z
N12 24893
Temperature seasonal anomaly (deg C)
3
2
1
0
−1
−2
CSIRO Marine Research
-21
-22
-23
-24
-25
-26
-27
-28
-29
-30
-31
-32
-33
-34
-35
-36
108 109 110 111 112 113 114 115 116 117

Ingredients

- Multi-layer shallow-water models;
- Exhaustive linear stability analysis by the collocation method;
- High-resolution numerical simulations of nonlinear evolution with new-generation finite-volume code.

Workflow

- Choose a model: 1.5 or 2 -layer (or more!);
- Choose bathymetry;
- Choose balanced profiles of velocity/interface;
- Analyse linear stability: unstable modes, growth rates;
- Initialise nonlinear simulations with the unstable modes, study saturation;
- Look how instabilities manifest themselves in initial-value problem.

Typical configuration

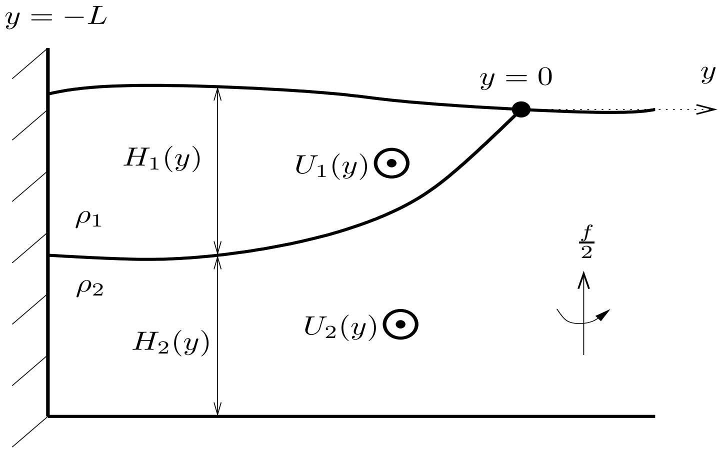

RSW equations with coast (no bathymetry)

Equations of motion:

$$\begin{aligned} u_t + uu_x + vu_y - fv + gh_x &= 0, \\ v_t + uv_x + vv_y + fu + gh_y &= 0, \\ h_t + (hu)_x + (hv)_y &= 0. \end{aligned} \qquad (1)$$

Boundary conditions:

$$H(y) + h(x,y,t) = 0, \quad D_t Y_0 = v \quad at \quad y = Y_0 \ , \qquad (2)$$

where $Y_0(x,t)$ is the position of the free streamline, D_t is Lagrangian derivative.

Balanced flows:

$u = U(y)$, $v = 0$, and $h = H(y)$,

$$U(y) = -\frac{g}{f} H_y(y) \tag{3}$$

exact stationary solution.

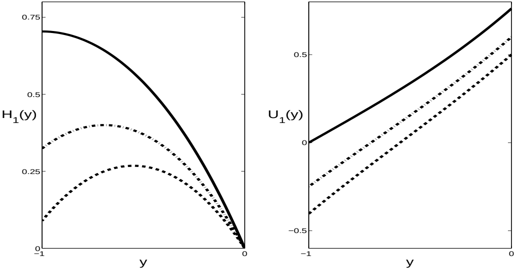

Figure: Examples of the basic state heights (left) and velocities (right) for constant PV flows with $U_0 = -sinh(-1)/cosh(-1)$ (thick line), $U_0 = 1/2$ (dotted) and a zero PV flow (dash-dotted)

Non-dimensional linearized system:

$$\begin{aligned} u_t + Uu_x + vU_y - v &= -h_x, \\ v_t + Uv_x + u &= -h_y, \\ h_t + Uh_x &= -(Hu_x + (Hv)_y). \end{aligned} \tag{4}$$

Linearized boundary conditions:

- $$Y_0 = -\frac{h}{H_y}\bigg|_{y=0}, \tag{5}$$
- continuity equation evaluated at $y = 0$.

The only constraint is regularity of solutions at $y = 0$.

PV of the mean flow

$$Q(y) = \frac{1 - U_y}{H(y)}, \tag{6}$$

Geostrophic equilibrium $\Rightarrow$

$$H_{yy}(y) - Q(y)H(y) + 1 = 0, \ \textit{with} \begin{cases} H(0) = 0 \\ H_y(0) = -U_0, \end{cases} \tag{7}$$

$U(0) = U_0$ is the mean-flow velocity at the front.

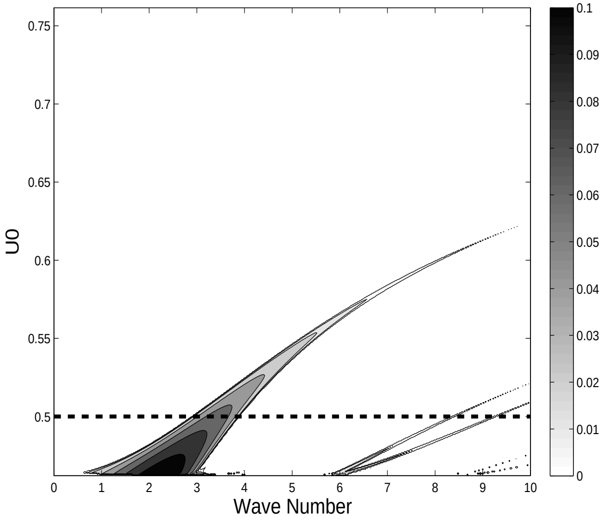

Figure: Stability diagram in the $(\frac{U_0}{fL}, k)$ plane for the constant PV current. Values of the growth rates in the right column.

Dispersion diagram: stable flow

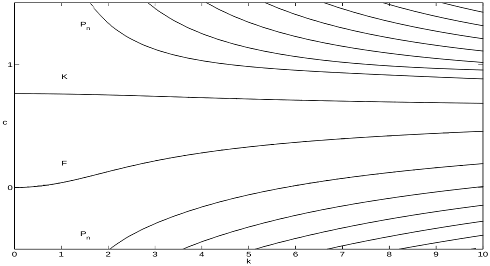

Figure: Dispersion diagram for $U_0 = -sinh(-1)/cosh(-1)$ and $Q_0 = 1$.

Dispersion diagram: unstable flow

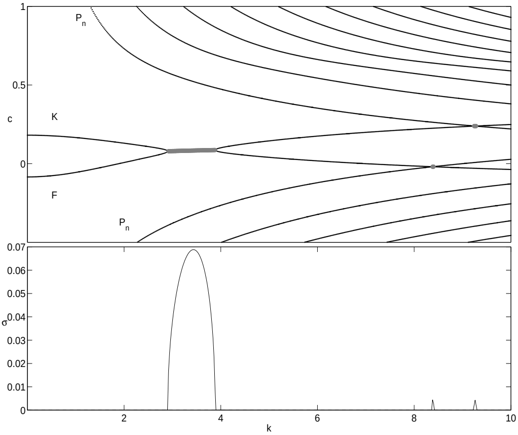

Figure: Dispersion diagram for $U_0 = 0.5$ and $Q_0 = 1$. Crossings of the dispersion curves in the upper panel correspond to instability zones in the lower panel.

The most unstable mode: Kelvin-Frontal resonance

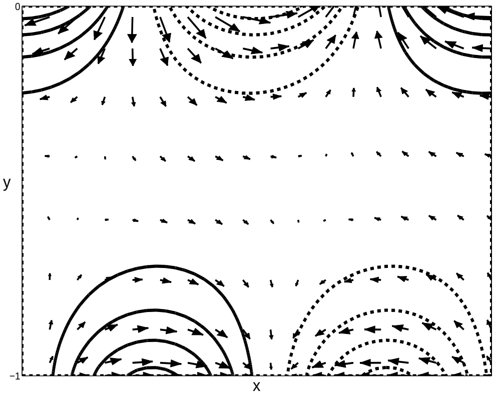

Figure: Height and velocity fields of the most unstable mode $k = 3.5$.

Saturation of the primary instability

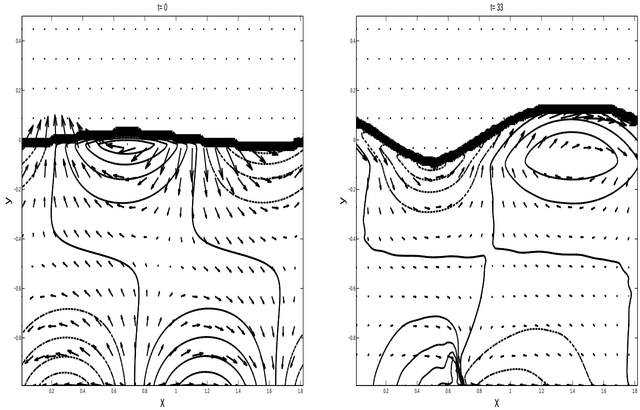

Figure: Height and velocity fields of the perturbation at $t = 0$ (left) and $t = 30$ (right). Kelvin front is clearly seen at the bottom of the right panel.

Kelvin wave breaking

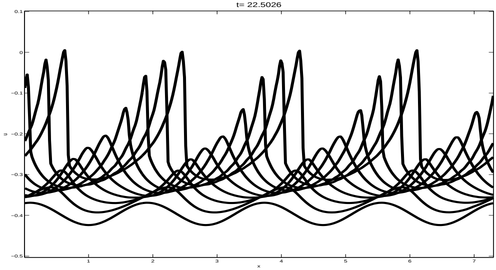

Figure: Evolution of the tangent velocity at $y = -L$ (at the wall) for $t = 0, 2.5, 5, 7.5, 10, 12.5, 15, 17.5, 20, 22.5$ (from lower to upper curves)

Secondary instability

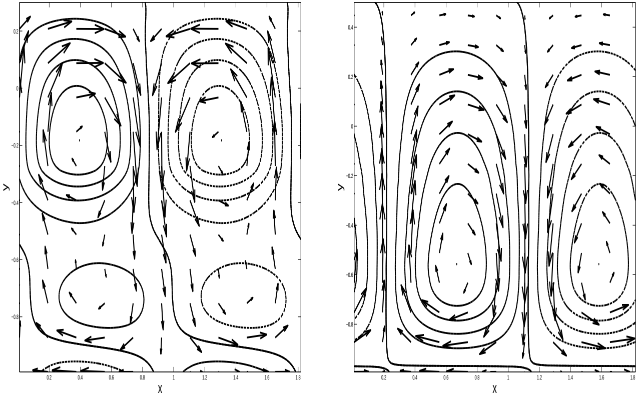

Figure: Height and velocity fields of the secondary perturbation at $t = 335$, $t = 500$ (right).

Reorganization of the mean flow

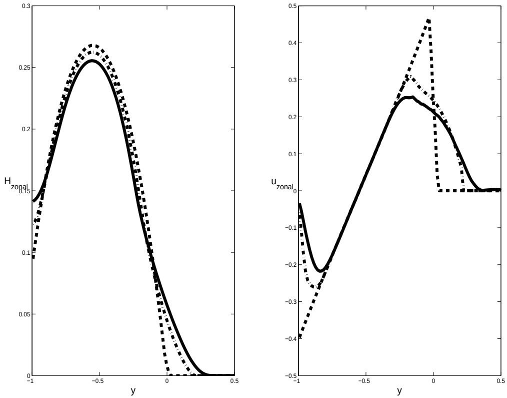

Figure: Evolution of the mean zonal height (left) and mean zonal velocity (right): Initial state $t = 0$ (dashed line), primary unstable mode saturated at $t = 40$ (dash-dotted line), late stage $t = 300$ (thick line).

Stability diagram of the reorganized flow

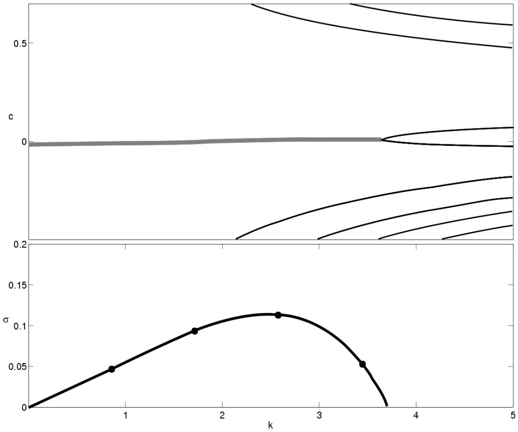

Figure: Dispersion diagram of the eigenmodes corresponding to the basic state profile of the flow at $t = 335$, at the beginning of the secondary instability stage (see Fig. 9).

Most unstable mode of the reorganized flow

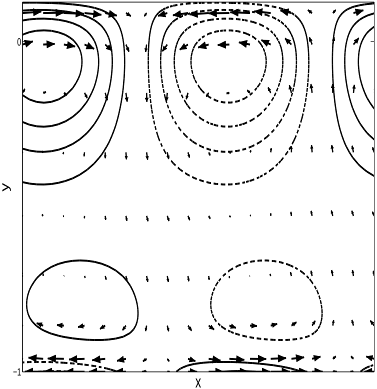

Figure: Height and velocity fields of the most unstable mode of figure 10 for $k = k_0$. Only one wavelenght is plotted. Note the similarity with the mode observed in the simulation, Fig. 8

Instability in Cauchy problem

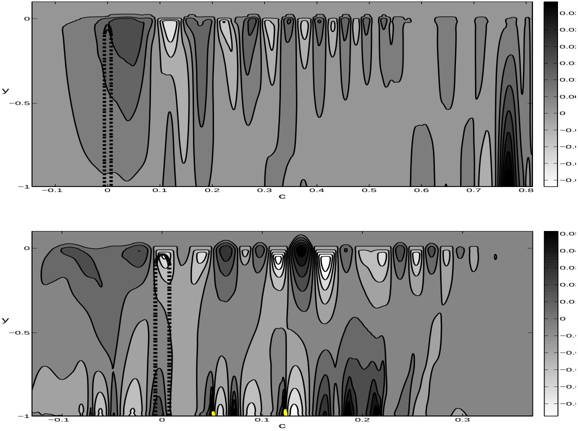

Figure: $y - c$ diagram of the height field at $t = 45$ of the development of initially localised perturbation (dotted) for linearly stable (upper) and unstable (lower) current. Phase-locking of frontal and Kelvin waves in the lower panel

Equations of motion

$$
\begin{aligned}
D_j u_j - f v_j &= -\frac{1}{\rho_j}\partial_x \pi_j, \\
D_j v_j + f u_j &= -\frac{1}{\rho_j}\partial_y \pi_j, \\
D_j h_j + \nabla \cdot (h_j \mathbf{v_j}) &= 0,
\end{aligned} \tag{8}
$$

$j = 1, 2$: upper/lower layer, (x, y), $h_j(x, y, t)$ - depths of the layers, π_j, ρ_j - pressures, densities of the layers,

$$
\nabla \pi_j = \rho_j g \nabla (s^{j-1} h_1 + h_2), \ s = \rho_1/\rho_2. \tag{9}
$$

Stationary solutions

Balanced flow with depths $H_j(y)$ and velocities $U_j(y)$:

$$\partial_y H_j = (-1)^{j-1} \frac{f}{g'}(U_2 - s^{j-1} U_1), \qquad (10)$$

Linearization/nondimensionalization:

$$\begin{aligned} \partial_t u_j + U_j \partial_x u_j + v_j \partial_y U_j - v_j &= -\partial_x (s^{j-1} h_1 + h_2), \\ \partial_t v_j + U_j \partial_x v_j + u_j &= -\partial_y (s^{j-1} h_1 + h_2), \\ \partial_t h_j + U_j \partial_x h_j + H_j \partial_x u_j &= -\partial_y (H_j v_j). \end{aligned} \qquad (11)$$

Boundary conditions

- Upper layer: same as in 1.5-layer case,
- Lower layer: for harmonic perturbations

$$(u_j(x,y), v_j(x,y), h_j(x,y)) = (\tilde{u}_j(y), \tilde{v}_j(y), \tilde{h}_j(y))\, e^{i(kx-\omega t)}, \quad (12)$$

Filtering of outer inertia-gravity waves, decay condition:

$$\partial_y(sh_1 + h_2) = -k(sh_1 + h_2) \text{ at } y = 0.$$

Key parameters:

U_0, the non-dimensional velocity of the upper layer at the front location $y = 0$, equivalent to Rossby number, aspect ratio $r = H_1(-1)/H_2(-1)$, and stratification $s = \rho_1/\rho_2$.

Configurations considered:

- Bottom layer: initially at rest ($U_2 = 0$),
- Upper layer: with constant PV.

Two classes of flows: barotropically stable/unstable, i.e. stable/unstable in the 1.5 - layer limit.

Barotropically stable case

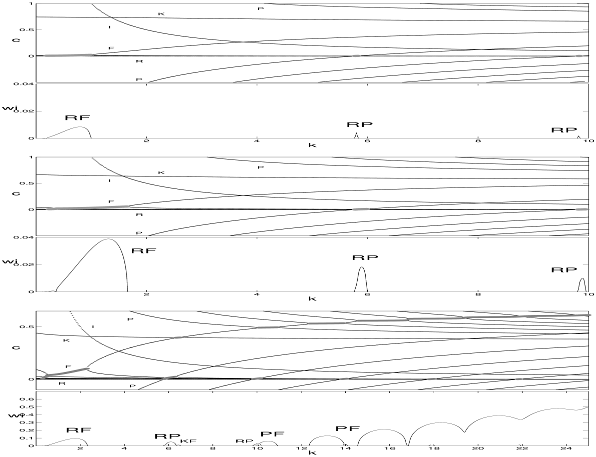

Figure: Dispersion diagrams for $s = .5$. (a) $r = 10$, (b) $r = 2$, (c) $r = 0.5$. Horizontal scale of the bottom panel shrinked to show short-wave KH instabilities.

Barotropically unstable case

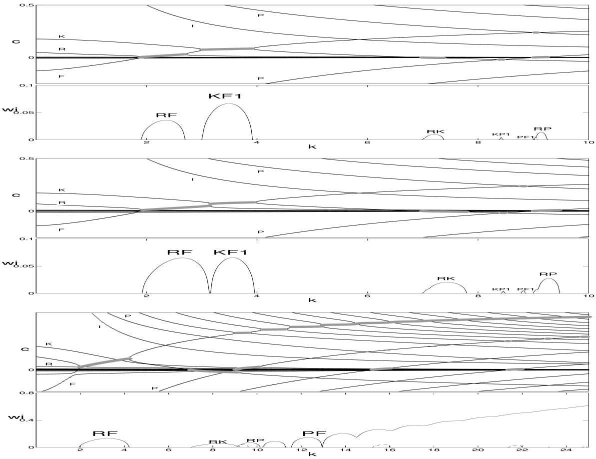

Figure: Dispersion diagrams for $s = 0.5$ and for $R_d = 1$. (a) $r = 10$, (b) $r = 5$, (c) $r = 2$. The horizontal scale of the panels shrinked to show short-wave KH instabilities.

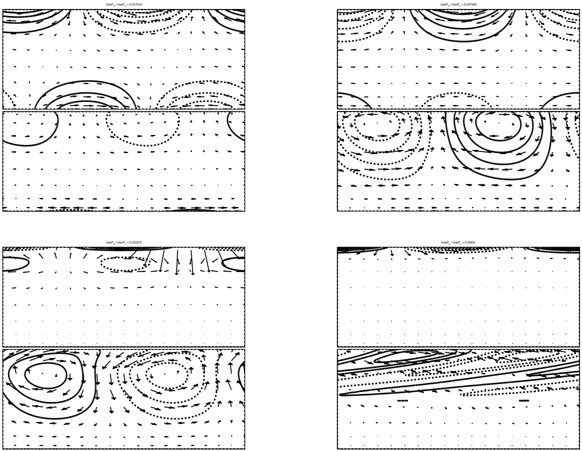

Figure: Typical unstable modes(left to right, top to bottom): KF1, RF, RP, PF.

Scenario of development of the baroclinic RF instability as follows from DNS

1. Upper layer: frontal wave evolves into a series of monopolar vortices at certain spacing due to vortex lines clipping and reconnection following formation of Kelvin fronts
2. Lower layer: Rossby wave develops a series of vortices of alternating signs
3. Lower-layer dipoles drive the vortex out of the shore and are at the origin of the detachment.

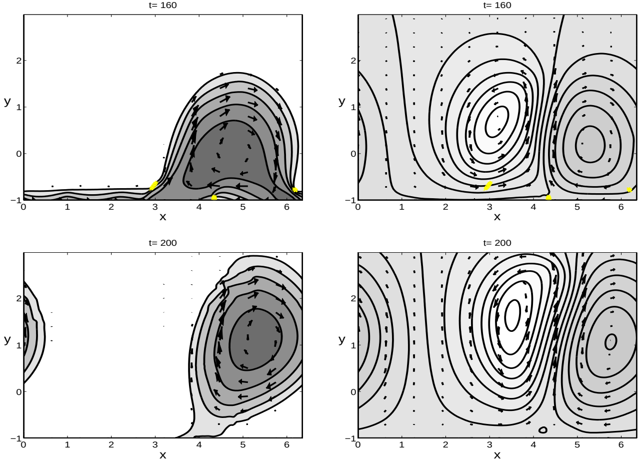

Figure: Levels of $h_1(x, y, t)$ in the upper layer (left) and isobars of $\pi_2(x, y, t)$ in the lower layer (right) at $t = 150$ and 200 for the development of the unstable RF mode superposed on the basic flow with a depth ratio $r = 2$.

Energetics

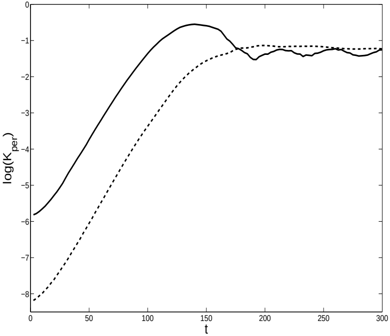

Figure: Logarithm of the kinetic energy K_{per} of the perturbation for the unstable mode in the upper layer (thick) and in the lower layer (dashed).

Kelvin front and dissipation during development of RF instability

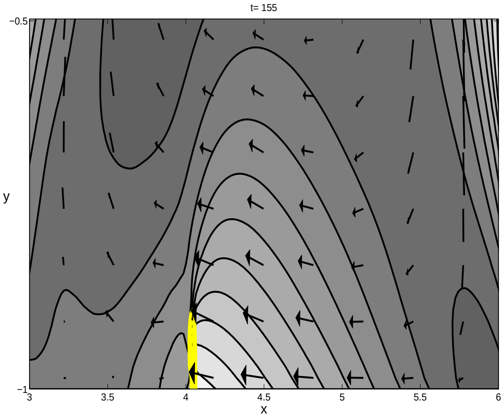

Figure: Before detachment: zoom of the wall region.

Structure of the detached vortex 1

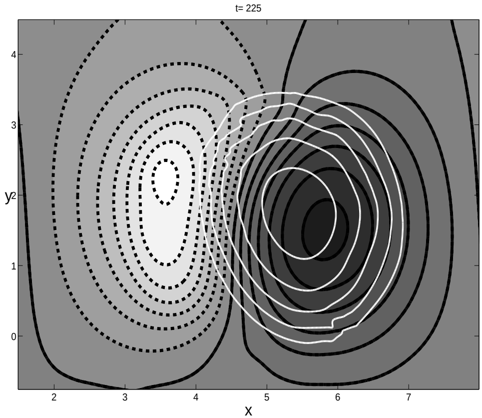

Figure: Isobars of $\pi_1(x, y, t)$ in the upper layer (white lines) and $\pi_2(x, y, t)$ in the lower layer (dark lines) at $t = 250$. Dark (light) background: anticyclonic (cyclonic) region.

Structure of the detached vortex 2

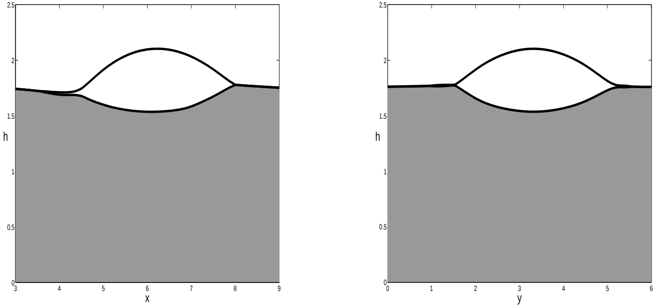

Figure: The x (left) and y (right) cross-sections of the detached vortex at $t = 300$

Evolution of the total energy

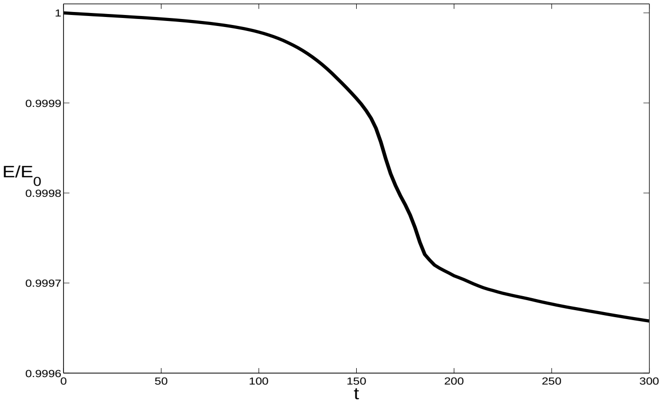

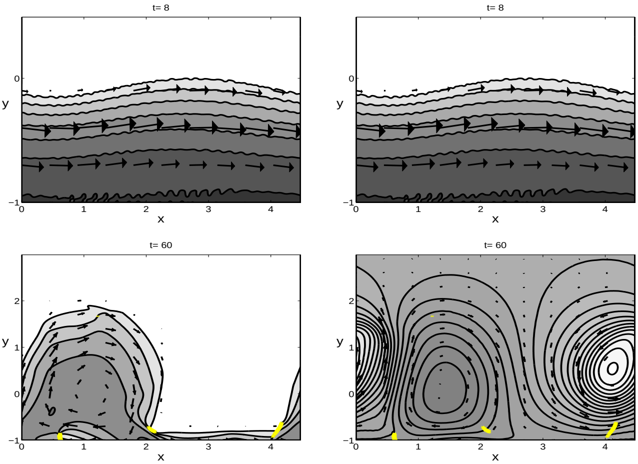

Figure: Levels of $h_1(x, y, t)$ in the upper layer (left) and isobars of $\pi_2(x, y, t)$ in the lower layer (right) at $t = 20$ and 60 for the development of the unstable RF mode superposed on the basic flow with a depth ratio $r = 0.5$.

Energetics

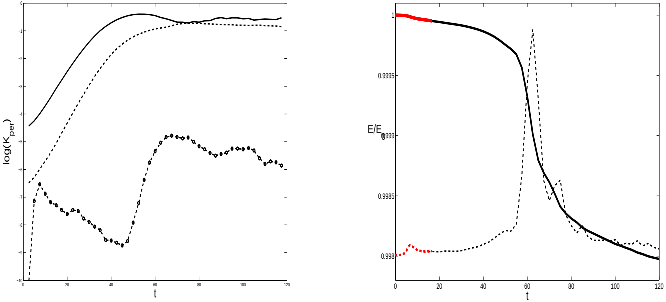

Figure: Left -logarithm of the kinetic energy of the perturbation for mode $k = k_0$ in the upper layer (solid) and in the lower layer (dashed), and for the sum of modes with $k > 10\ k_0$ (dashed-dotted). Right - time-dependence of the total energy (thick line) and the dissipation rate (dashed line) for the evolution of the instability

Loss of hyperbolicity

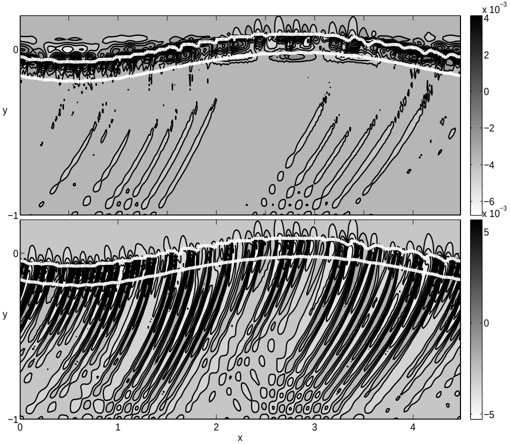

Figure: Contours of $\pi_1(x, y, t)$ (upper panel) and $\pi_2(x, y, t)$ (lower panel) with mean zonal flow filtered out at $t = 20$, with a depth ratio $r = 0.5$. The white lines indicate the boundaries of non-hyperbolic domains.

- Exhaustive linear stability analysis of coastal currents/oucropping fronts performed,
- Physical nature of all instabilities as resonances between various eigenmodes established,
- Nonlinear evolution of leading instabilities simulated with new high-resolution finite-volume code,
- An essential role of Kelvin fronts (breaking Kelvin waves) in reorganization of the flow and coherent structure formation highlighted,
- A mechanism of vortex detachment from the unstable baroclinic coastal current is identified,
- (Non-) Influence of short-scale shear instabilities understood.

References

Presentation is based on

- J. Gula and V. Zeitlin, "Instabilities of buoyancy-driven coastal currents and their nonlinear evolution in the two-layer rotating shallow water model. Part 1. Passive lower layer", *J. Fluid Mech.*, **659**, 69 - 93 (2010).
- J. Gula, V. Zeitlin and F. Bouchut, "Instabilities of buoyancy-driven coastal currents and their nonlinear evolution in the two-layer rotating shallow water model. Part 2. Active lower layer" *J. Fluid Mech.*, **665**, 209 - 237 (2010).